Proceedings of the CAS–CERN Accelerator School: Free Electron Lasers and Energy Recovery Linacs, Hamburg, Germany, 31 May–10 June 2016, edited by R. Bailey, CERN Yellow Reports: School Proceedings, Vol. 1/2018, CERN-2018-001-SP (CERN, Geneva, 2018)

Undulator Technology

J. Pflueger
European XFEL GmbH, Schenefeld, Germany

Abstract
Since the 1970s undulators are used in storage rings and free-electron lasers as sources of intense radiation. This tutorial gives an elementary introduction and describes the principles as well as electromagnetic, superconducting and permanent magnet technologies, which are used in practice. Special emphasis is put on permanent magnet technology, which is most developed and used in most practical applications. An overview illustrated by many examples of the state of the art is given.

Keywords
Undulators; free-electron lasers; permanent magnets.

1 Introduction

The word ‘undulator’ originates from the Latin word for wave, ‘unda’. Its meaning is thus ‘wave maker’. By using a series of magnet poles with the same lengths and strengths but alternating field directions an ultra-relativistic electron beam is forced on a wave like, wiggling but overall straight orbit as shown schematically in Fig. 1.

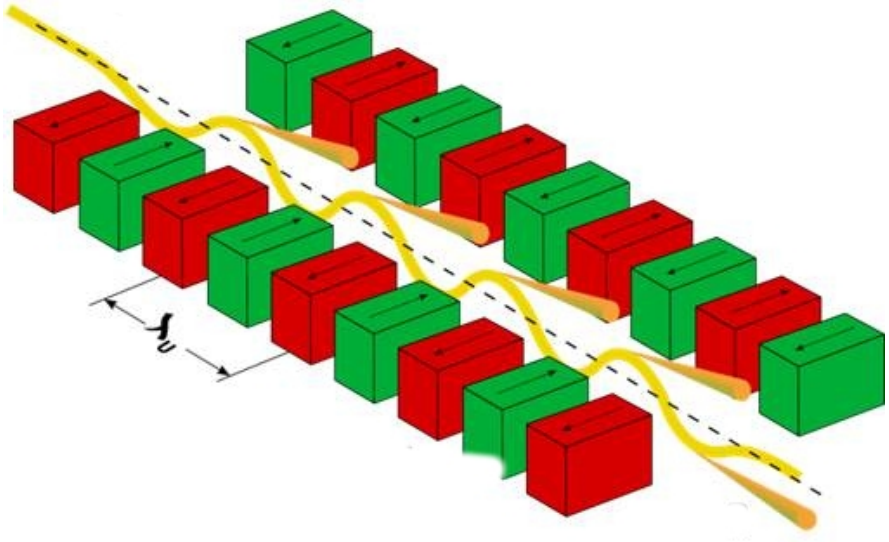

Fig. 1: Schematic of an undulator

Common and often used synonyms are ‘insertion device’ or ‘wiggler’. There are three technologies to create the periodic magnetic field: permanent magnet (PM), electromagnetic (EM) and superconducting (SC) technologies. They will be treated in this report. Typical device lengths are in the range of about 0.5 to 5 m. The development and use of undulators as intense sources of synchrotron radiation began in the late 1970s when first devices were developed for use in storage rings at the Budker Institute for Nuclear Physics (BINP) in Novosibirsk and the Lawrence Berkeley National Laboratory (LBNL) in co-operation with Stanford Synchrotron Radiation Laboratory (SSRL).

https://doi.org/10.23730/CYRSP-2018-001.55

In a storage ring an undulator requires a straight section of an appropriate length. Such straight sections were very rare at that time. Therefore since the 1990s, dedicated third-generation storage rings were developed, which were optimized to accommodate a large number of straight sections and provide space for many insertion devices. Nowadays large facilities like the European Synchrotron Radiation Facility, (ESRF), the Advanced Photon Source (APS), the Super Photon Ring-8 GeV, (Spring8) or the reconstructed Positron Electron Tandem Ring Anlage, (PETRA III) accommodate dozens of such devices with lengths up to 5 m. An early historic insertion device built at Deutsches Elektronen Synchrotron (DESY) in 1983 is shown in Fig. 2. It is the 2.3 m long W1 wiggler. It occupied the only straight section available at that time in the storage ring "Doppelringspeicher", (DORIS).

Fig. 2: The W1 wiggler in use at DESY/HASYLAB in the DORIS storage ring from 1983 to 2012

In the last 15 years X-ray free-electron lasers (XFELs) using the principle of self-amplified spontaneous emission (SASE) were developed. They require very long systems of undulators and generate soft and hard X-ray beams with extreme properties allowing for revolutionary new experimental techniques. Examples are the **F**ree Electron **Las**er in **H**amburg, (FLASH) at DESY, Germany, the Linac Coherent Light Source, (LCLS) in Stanford, USA or the **S**pring8 **A**ngstroem **C**ompact Free Electron **La**ser (SACLA) at Spring8 in Harima, Japan. All are already in operation since several years. New projects with even more improved properties are in construction at the European XFEL/DESY (EXFEL) in Schenefeld/Hamburg, Germany, SwissFEL at Paul Scherrer Institute (PSI) in Villingen, Switzerland and XFEL at the Pohang Accelerator Laboratory (PAL-XFEL) in Pohang, Korea.

Depending on beam parameters and radiation properties the lengths of undulator systems vary from 30 m for FLASH to about 220 m for EXFEL. Although the requirements and specifications are different, the undulator technology has a lot in common.

This contribution will give a basic understanding of undulator properties and evaluation criteria. For a deeper insight the books by Onuki/Elleaume [1], Clarke [2] and the *Handbook of Synchrotron Radiation* [3] treat many theoretical as well as practical aspects, which were omitted on purpose in this contribution on technology: calculation of emission properties, magnetic measurement techniques of insertion devices, magnet design and special insertion devices. The state of the art of undulator technology is illustrated by a number of examples.

2 Basics

2.1 Equations of motion

In this section some fundamental relations for commonly used key parameters are derived. The motion of an electron in a periodic field of an undulator is sketched in Fig. 3.

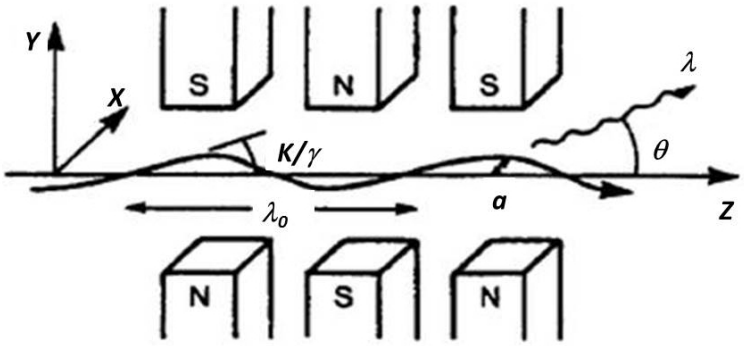

Fig. 3: Electron motion in an undulator

This figure also defines the coordinate system used in this contribution. The motion of a single electron in a magnetic field is controlled by the Lorentz equations:

$$\vec{F} = \frac{\mathrm{d}\vec{p}}{\mathrm{d}t} = m_0\gamma\frac{\mathrm{d}}{\mathrm{d}t}\vec{v} = m_0\gamma\begin{pmatrix}\ddot{x}\\ \ddot{y}\\ \ddot{z}\end{pmatrix} = e\left[\vec{v}\times\vec{B}\right] = e\cdot\begin{pmatrix}v_yB_z - v_zB_y\\ v_zB_x - v_xB_z\\ v_xB_y - v_yB_x\end{pmatrix}. \quad (1)$$

Here $\vec{F}$ is the force acting on an electron, $\vec{p}$ its momentum and $\vec{v}$ its velocity vector. m_0 is the electron rest mass, $\gamma$is the kinetic energy in units of the rest mass and e its charge. $\vec{B}$ is the vector of the magnetic field.

2.2 Transverse motion

For the motion in a planar undulator Eq. (1) is solved by making the assumption for a planar field:

$$\vec{B} = \begin{pmatrix}0\\ B_0\sin\left(\frac{2\pi}{\lambda_0}z\right)\\ 0\end{pmatrix}, \quad (2)$$

where λ_0 is the period length of the field and B_0 its amplitude. B_x, $B_z = 0$. $\vec{B}$ is a purely transverse field which varies along z, the direction of propagation. The initial conditions are

$$v_x,\ v_y = 0;\ v_z = \beta c\,, \quad (3)$$

where c is the speed of light and the following relations are used:

$$\beta = \sqrt{1-\frac{1}{\gamma^2}} \cong 1-\frac{1}{2\gamma^2};\quad \gamma = \frac{E_{\mathrm{Kin}}}{m_0c} \gg 1\,. \quad (4)$$

For multi-GeV beams this condition is very well satisfied and γ is in the order of many times 10^3. In practice for most undulators the period length, λ_0, is in the range of 10 to 400 mm and B_0 of the order of 1–2 T. As will be shown quantitatively below, transverse velocities are small enough so that the small-angle approximation can be made:

$$\frac{v_x, v_y}{\beta c} = x', y' << 1\,. \quad (5)$$

Then Eq. (1) can be simplified:

$$\begin{aligned} \ddot{x} &= -\frac{e}{\gamma m_0} v_z B_y \,, \\ \ddot{y} &= 0 \,, \\ \ddot{z} &= \frac{e}{\gamma m_0} v_x B_y \cong 0 \,. \end{aligned} \tag{6}$$

For the deflection angle x' it can be solved by integration:

$$x'(z) = \frac{v_z(z)}{\beta c} = -\frac{e}{\gamma m_0 c} \int_{-\infty}^{z} B_y(z')\mathrm{d}z' \,. \tag{7}$$

The integral

$$\int_{-\infty}^{z} B_y(z')\mathrm{d}z' = \boldsymbol{I}1(z) \tag{8}$$

is called the first field integral and can be calculated using measured field data, if available.

For the sinusoidal field as assumed in Eq. (2),

$$x'(z) = \frac{eB_0\lambda_0}{\gamma\ m_0 c 2\pi} \cos\left(\frac{2\pi}{\lambda_0} z\right) = \frac{K}{\gamma} \cos\left(\frac{2\pi}{\lambda_0} z\right) \tag{9}$$

is obtained, where

$$K = \frac{eB_0\lambda_0}{m_0 c 2\pi} = 0.0934\ B_0[\mathrm{T}] \cdot \lambda_0[\mathrm{mm}] \tag{10}$$

defines the undulator K-parameter for a purely sinusoidal field as assumed in Eq. (2). The maximum excursion angle of the electron beam is given by K/γ. For non-sinusoidal but periodic B_y fields it is given by

$$K_{\mathrm{Def}} = \mathrm{Max}\left(\frac{e}{m_0 c} \boldsymbol{I}1(z) \right), \tag{11}$$

where the suffix 'Def' marks the definition using the deflection criterion. Real fields of undulators are periodic, but in general contain higher harmonics and therefore the K-parameter differs from the definition given in Eq. (10).

The electron trajectory in the X–Z plane is obtained by a second integration of Eq. (9):

$$x(z) = -\frac{e}{\gamma m_0 c} \int_{-\infty}^{z} \left(\int_{-\infty}^{z'} B_y(z'')\mathrm{d}z'' \right) \mathrm{d}z' \,. \tag{12}$$

Here the second field integral is defined as

$$\boldsymbol{I}2(z) = \int_{-\infty}^{z} \left(\int_{-\infty}^{z'} B_y(z'')\mathrm{d}z'' \right) \mathrm{d}z' \,. \tag{13}$$

For the sinusoidal field of Eq. (2), the result is

$$x(z) = -\frac{eB_0\lambda_0^2}{\gamma m_0 c\, 4\pi^2} \cdot \sin\left(\frac{2\pi}{\lambda_0} z\right) = -\frac{K}{\gamma}\ \frac{\lambda_0}{2\pi} \cdot \sin\left(\frac{2\pi}{\lambda_0} z\right), \tag{14}$$

so that the amplitude of the trajectory oscillation, A, is given by

$$A = \frac{K}{\gamma}\ \frac{\lambda_0}{2\pi} \,. \tag{15}$$

A short comment on non-monochromatic field contributions: Eqs. (10) and (15) are commonly used and give estimates better than 10–15%. Details, however, depend on the presence of higher field harmonics, which in turn depend on technological details such as the minimum gap and the period length λ_0 as well as on dimensions of the magnetic active parts. It therefore needs a careful analysis if higher precision is required.

2.3 Longitudinal motion

In a magnetic field the total velocity of an electron is constant. This connects the longitudinal and transverse motions:

$$v_y^2 + v_z^2 = (\beta c)^2 \,. \tag{16}$$

Using Eqs. (7) and (9), the evolution of the longitudinal speed can be written:

$$v_z = \sqrt{(\beta c)^2 - v_x^2} \cong \beta c\left(1 - \frac{v_x^2}{2\cdot(\beta c)^2}\right) = c\beta\left[1 - \frac{K^2}{4\gamma^2} - \frac{K^2}{4\gamma^2}\cos\left(\frac{4\pi}{\lambda_0}z\right)\right]. \tag{17}$$

This result shows two consequences:

1. The average longitudinal speed is reduced since the oscillations in the undulator increase the path length. This can be accounted for using $\bar{\beta}$ defined as

$$\bar{\beta}=\beta\left[1 - \frac{K^2}{4\gamma^2}\right]. \tag{18}$$

2. In addition, the longitudinal speed is modulated by the factor $\frac{K^2}{4\gamma^2}\cos\left(\frac{4\pi}{\lambda_0}z\right)$ with two oscillations per period λ_0. As compared to Eq. (9), the longitudinal amplitude is reduced by $\frac{K}{4\gamma}$.

Equation (17) can be rewritten:

$$v_z = \mathrm{c}\left[\bar{\beta} - \frac{K^2}{4\gamma^2}\cos\left(2\cdot\frac{2\pi}{\lambda_0}z\right)\right]. \tag{19}$$

2.4 Slippage, optical phase and phase errors

Light travels at light speed c. An electron in an undulator travels at lower average speed given by $\bar{\beta}c$. This gives rise to an effect called 'slippage', which is explained in Fig. 4. The black full line sketches the oscillating trajectory of an electron in an undulator. The time for light to travel the distance from A to B, one period length, λ_0, is given by $t_c = \frac{\lambda_0}{c}$. In that time the electron travels only the distance $\frac{\lambda_0}{c}\bar{\beta}c$. The difference is called 'slippage'. Using Eqs. (4) and (18) and neglecting the term proportional to $\frac{1}{\gamma^4}$ the slippage of one period is given by

$$\Delta = \lambda_0\left(1 - \bar{\beta}\right) = \frac{\lambda_0}{2\gamma^2}\left(1 + \frac{K^2}{2}\right). \tag{20}$$

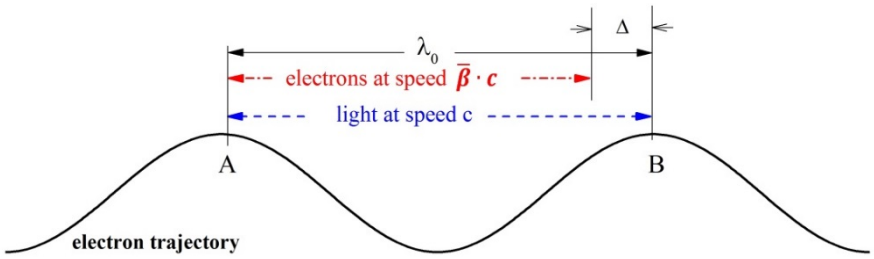

Fig. 4: Slippage in an undulator

Since the slippage in all periods of an ideal undulator is the same, the light emitted by different periods constructively interferes at the wavelength given by Eq. (20). It is therefore more common to rewrite Eq. (20) using the radiation wavelength, λ_{Rad}:

$$\lambda_{\mathrm{Rad}} = \frac{\lambda_0}{2\gamma^2}\left(1 + \frac{K^2}{2}\right), \tag{21}$$

which is the well-known resonance condition for the first harmonic of an undulator.

2.5 Optical phase

The accumulated slippage in a magnetic field extending from z_0 to z is given by

$$\Delta(z) = \int_{z_0}^{z} \big(c - v_z(z')\big)\mathrm{d}z'. \tag{22}$$

The optical phase is the total slippage normalized to $\frac{\lambda_{\mathrm{Rad}}}{2\pi}$ and defined as

$$\varphi(z) = 2\pi \frac{\Delta(z)}{\lambda_{\mathrm{Rad}}}. \tag{23}$$

Combining Eqs. (7), (17), (21) and (22), one obtains the optical phase for $B_y(z)$

$$\varphi(z) = 2\pi \frac{\Delta(z)}{\lambda_{\mathrm{Rad}}} = \frac{2\pi}{\lambda_0(1+\frac{K^2}{2})} \left(z + \left(\frac{e}{m_0}\right)^2 \int_{-\infty}^{z} \left(\int_{-\infty}^{z''} B_y(z')\mathrm{d}z' \right)^2 \mathrm{d}z'' \right). \tag{24}$$

This result can again be applied to measured magnetic field data $B_y(z)$. The normalization to λ_{Rad}, the first harmonic, eliminates γ and leads to an energy-independent form.

The double integral

$$\mathrm{PI}(z) = \int_{-\infty}^{z} \left(\int_{-\infty}^{z''} B_y(z')\mathrm{d}z' \right)^2 \mathrm{d}z'' \tag{25}$$

is commonly called ‘Phase Integral’.

2.6 Phase errors

The optical phase is very important for evaluating the quality of an undulator in terms of its emission properties. This is understood by a qualitative argument: field errors lead to changes in the transverse velocity and thus result in changes of the longitudinal velocity as seen by Eq. (17). This will perturb the phase advance per period of 2π and lead to a phase mismatch of the radiation emitted by different periods and the quality of the produced radiation will be degraded. The criterion which controls this degradation is the phase jitter, also called phase error. It is defined as the RMS difference between the ideal and the actual phases on the poles of an undulator as determined by Eq. (24).

This can be written as

$$\mathrm{PJ} = \frac{1}{N} \sum_{i=1}^{N} (i \cdot \pi - \varphi(z_i))^2 . \tag{26}$$

Here i labels the poles and z_i are the corresponding positions. The nominal phase advance per pole is π. Phase errors are a reliable quality criterion for the evaluation of emission properties of an undulator. For spontaneous emission of undulators in synchroton radiation (SR) sources this was established by Walker; see Ref. [4]. For undulators in SASE-FELs, Li *et al.* [5] have made a thorough investigation. Today magnetic measurement and tuning techniques allow for RMS phase jitters of 1° or 0.0175 rad or even less. However, this should not be overstressed. Such a small PJ is only needed if an undulator will be operated at a high harmonic, which is often the case in SR sources, see Ref. [4]. In contrast, SASE-FELs are operated on the first harmonic only. Here a PJ of 11° or 0.192 rad is sufficient. It should be mentioned that the phase-error criterion avoids the unnecessary over specification of very small peak field errors, which is sometimes found. As shown in Ref. [5] some errors at the proper location are tolerable.

2.7 Demonstration and example

The relations derived in the previous sections are illustrated by two examples in Fig. 5. A short model of 20 periods of a XFEL U40 undulator with λ_0 = 40 mm and B_0 = 1 T is shown. The *K*-parameter is 3.72. For simplicity and explanation this short model field rather than that of a real 5 m long undulator with 120 full periods was selected.

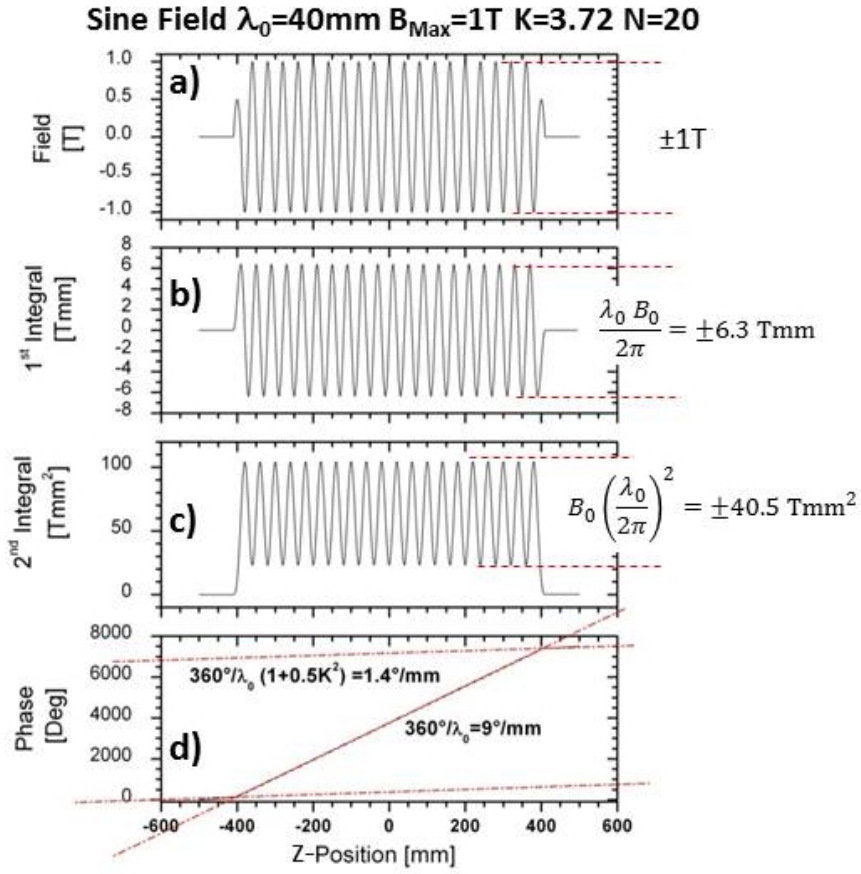

Fig. 5: Field, first, second field integrals and phase integral for a short model with 20 periods

Figure 5(a) shows the field with an amplitude of ±1 T. The first field integral with an amplitude of ±6.3 T mm calculated using Eqs. (7) and (9) is shown in Fig. 5(b). The amplitude of the second field integral, Eqs. (12) and (13), is ±40.5 T mm2 and shown by Fig. 5(c). Finally, Fig. 5(d) shows the phase advance and illustrates Eq. (24). On both ends, outside the undulator, there is zero field and the phase evolution is that in free space represented by a straight line with a slope given by $\frac{360^\circ}{\lambda_0(1+0.5K^2)} = 1.4^\circ/\text{mm}$. Inside the undulator, the phase advance is 360° per period or a slope of $\frac{360^\circ}{\lambda_0} = 9^\circ/\text{mm}$. It is seen that over the 20 periods the phase advance is about 7200°.

The measured phase errors of a typical XFEL U40 are shown in Fig. 6. The phase error on each pole i is calculated using Eqs. (24) and (26). There are about 240 poles. The phase errors on all these poles were measured at six different gaps and their RMS values are shown in Fig. 6.

It is seen that there is some systematic variation along the undulator. Its amplitude changes with gap. The smallest value is at 14 mm gap leading to an RMS error of 1.77°. The results show that the phase error of this undulator is well within the XFEL specifications, which require an RMS phase error of less than 8°.

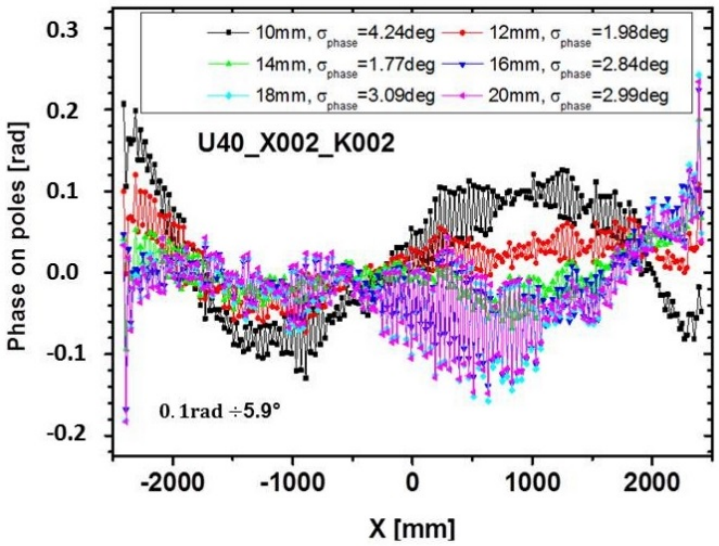

Fig. 6: Phase errors of a XFEL U40 measured at different gaps

3 Hardware technology

3.1 Technological limitations

EM, SC and PM technologies are used for the technical realization of periodic fields in undulators. In this section their Pros and Cons as well as technological limits will be discussed.

The first two, EM and SC technologies, are magnet systems excited by currents in conductors. Apart from the much higher currents and current densities in SC systems there is no fundamental difference between an EM and a SC system. In an EM system it is the current in a copper conductor, in a SC system a typical wire material is NbTi. Both need a sufficiently large cross-section to carry the total excitation current. This marks a difference to PM systems, where PM material based on SmCo or NdFeB with a remanent field of 0.9–1.25 T is used. Homogeneous PM material can be described by a surface current given by

$$j_{\mathrm{Surface}} = \frac{M}{\mu_0} \ , \tag{27}$$

where M is the magnetization and $\mu_0 = 1.256 \times 10^{-6}\ \mathrm{V\,s/A\,m}$ the vacuum permeability. For a remanent field of 1.25 T a surface current of about 10^6 A/m results. This results in a fundamental difference in the scaling properties of EM and PM systems, which is explained in Fig. 7. Here the scaling properties of a simple EM and a PM dipole system using an iron yoke are investigated if all dimensions are scaled down, i.e. divided by a factor a, and the scaled down systems are required to have the same field in the gap.

For the original EM system the field in the gap is obtained by integrating the magnetic field strength, H, around a closed path containing the enclosed current as indicated in Fig. 7. The iron contribution is negligible due to its very large permeability and only the field in the gap contributes.

$$\oint \ H\mathrm{d}s = \frac{B_{\mathrm{Gap}} \cdot \mathrm{Gap}}{\mu_0} = j_{\mathrm{Area}} A = I \ \rightarrow \ B_{\mathrm{Gap}} = \frac{j_{\mathrm{Area}} A}{\mathrm{Gap}} \mu_0 \ . \tag{28}$$

A is the cross-section of the conductor, j_{Area} is the current density and I is the total enclosed current. For the scaled down system the linear dimensions are divided by the scaling factor a, $\mathrm{Gap}_{\mathrm{Scaled}} = Gap/a$ and $A_{\mathrm{Scaled}} = A/a^2$. This leads to the requirement for the current density:

$$j_{\mathrm{Area,Scaled}} = j_{\mathrm{Area}} \cdot a \tag{29}$$

if the requirement $B_{\mathrm{Gap}} = B_{\mathrm{Gap,Scaled}}$ needs to be fulfilled. So, for the system scaled down by $a > 1$, the current density needs to increase proportional to a. There are, however, technical limits for current densities, as will be shown below.

A PM system behaves differently. Integration of H along a closed path results in

$$\oint Hds = \frac{B_{\mathrm{Gap}}\mathrm{Gap} + l_{\mathrm{m}}B_{\mathrm{m}}}{\mu_0} = j_{\mathrm{Surface}}l_{\mathrm{m}} = \frac{M}{\mu_0}l_{\mathrm{m}} = I\,. \tag{30}$$

The magnet is treated like an infinitely thin air coil of length l_{m} and the surface current density is given by Eq. (27). Since the flux in the gap and magnet, i.e. the number of field lines, is preserved, $B_{\mathrm{m}} = B_{\mathrm{Gap}}$,

$$B_{\mathrm{Gap}} = \frac{Ml_{\mathrm{m}}}{\mathrm{Gap}+l_{\mathrm{m}}} = \frac{M}{\frac{\mathrm{Gap}}{l_{\mathrm{m}}}+1}\,. \tag{31}$$

In this result only the geometric ratio $\mathrm{Gap}/l_{\mathrm{m}}$ determines the field, not the absolute coordinates. So, the fields of PM structures are invariant under a change of scale. The consequence of this scaling property is seen when the geometries are miniaturized: EM structures are limited by the current density for copper of $\lesssim 10\,\frac{\mathrm{A}}{\mathrm{mm}^2}$; for superconductors it may exceed 1500 $\frac{\mathrm{A}}{\mathrm{mm}^2}$ but the basic principle of limitation is the same. For a PM system such a limitation does not exist.

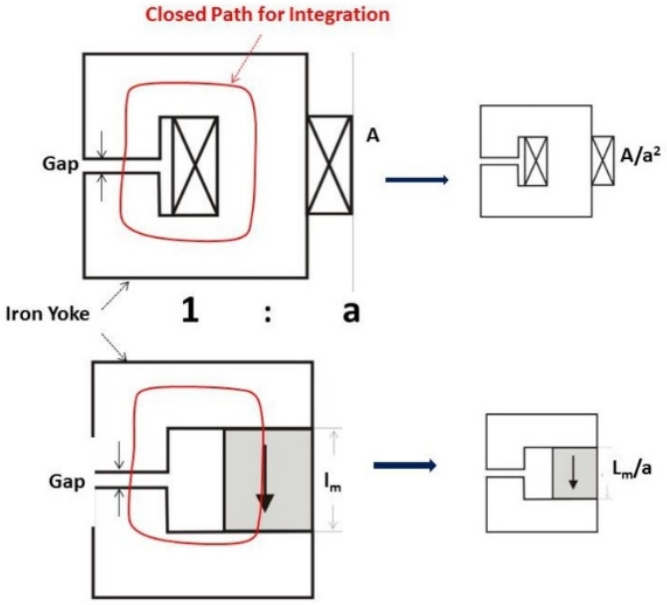

Fig. 7: Scaling properties of EM and PM systems

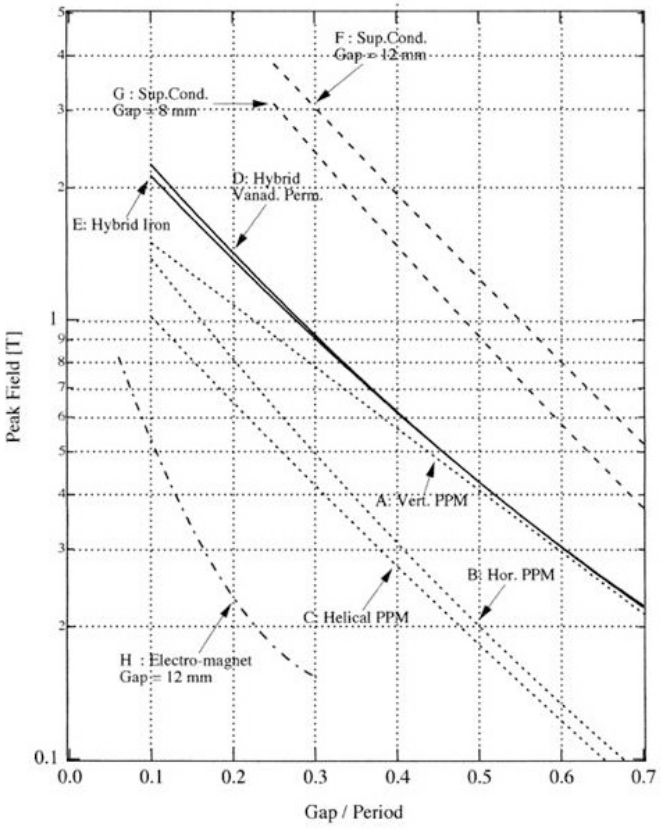

Fig. 8: Comparison of EM, SC and PM technologies

For illustration and without going into any design details, Fig. 8 shows a comparison of the peak field of undulators using EM, SC and PM technologies. The figure is taken from Ref. [6]. The scaling is gap/period, which is appropriate for PM. For EM and SC the comparison is made at gap = 12 mm. It is seen that EM shows the lowest values. A peak field of 0.8 T is only possible if the period length is about 200 mm. This is of practical use only for special cases.

SC offers the highest fields. At a gap of 12 mm a period length of about 50 mm would result in almost 4 T and at a period length of 17 mm still about 0.5 T is possible. For PM technology several curves are shown for different magnet designs, which will be explained below. They are somewhere in between EM and PM.

In summary, EM technology may be useful for undulators with long or even very long period lengths, $\lambda_0 > 200$ mm, and for very special applications. Its technology is well established and has much in common with classical EM magnets for accelerator applications.

SC has two regions: at periods larger than about 40 mm, fields of several Teslas may be reached. Wavelength shifters are such extreme applications, as will be shown below. There are numerous such long-period, high-field devices in operation in various laboratories. Typically, they have very few periods, sometimes only one. This technology is well established.

In contrast, the technology for short-period SC undulators is much more demanding, still under development and far away from being ‘state of the art’. At present there are only very few laboratories world-wide working on short-period SC undulators. There are, however, promising technological developments, which need time to get established. At period lengths down to 10–15 mm SC outperforms the other technologies but with decreasing difference the smaller the periods are.

PM technology is well established and is the workhorse technology for insertion devices. An estimated 90–95% of all devices are built in this way. Very large systems have been built in co-operation

with industrial suppliers. For example, the European XFEL requires 91 5 m long undulators with a total magnetic length of 455 m. Typical period lengths for PM undulators are 10–250 mm. In contrast to EM and SC undulators, PM technology has one important and obvious advantage: since a PM system is permanently excited there are no operation costs for electric power or cryogenics as for EM and SC systems and maintenance costs are low.

3.2 EM examples

Two examples for EM undulators will be explained. The first is shown in Fig. 9. It is the infrared/THz undulator for FLASH. It is a planar device with a very large period length of 400 mm. Water-cooled coils are wound around the poles, as can be seen schematically in the RADIA model in the upper left. The device has a gap of 40 mm, which is needed to guide the infrared radiation without losses. The maximum field at full excitation is 1.2 T. For FLASH operated at 1.2 GeV very intense coherent infrared radiation with wavelengths as long as 4.2 μm can be generated with this device. Operation cost should not be neglected: its power consumption at full excitation is 80 kW. At current electricity prices and 100% operation this amounts to around 400 €/day or 140 k€/year.

The second example is the EM helical undulator built for the APS and is shown in Fig. 10. It is a more sophisticated and rather exotic device. The cross-section is shown in the upper left part. There is a vertical structure for the B_y field similar to that in Fig. 9 but there is a second structure for the horizontal B_x field, which is displaced by a quarter period. The overall geometry is such that it allows for the insertion of a vacuum chamber with a very large horizontal aperture as required in storage rings and as shown in the upper left part of Fig. 10. Therefore, the B_x coils are split into an upper and a lower part. The period length is 125 mm, which is short for an EM undulator but the resulting field at 10.5 mm gap is only 0.3 T resulting in a K-parameter of 3.5. At the APS with 7 GeV this structure will create soft X-ray radiation around 500 eV. There is another speciality: the iron core of this device is laminated. This allows for operation of the coils with AC at 10 Hz rather than DC. So, the helicity of the field can be reversed quickly, which is important for studying magnetic phenomena.

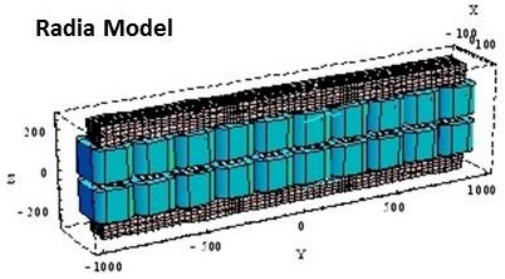

Gap	40 mm
Period length	400 mm
Pole length/width	100/140 mm
Number of full periods	9
Number of poles	44
End termination pattern	+1/8,-1/2,+1,...,-1,+1/2,-1/8
Iron yoke length	4.3 m
Maximum field/K-value	12 kG/49
Number of turns of central main coils	64
Conductor cross-section	8.5 × 8.5 mm², ∅ 5.3 mm bore
Maximum current density	8.7 A/mm²
First/second field integral	< 200 G cm, < 20 kG cm²
Maximum magnetic force	237 kN
Cooling water flow	100 l/min
Water temperature rise at 435 A	20 °C
Maximum temperature gradient (water cut-off)	0.4 °C/s
Maximum current	435 A
Voltage at 435 A	208 V
Maximum total power	87 kW
Total weight	4490 kg

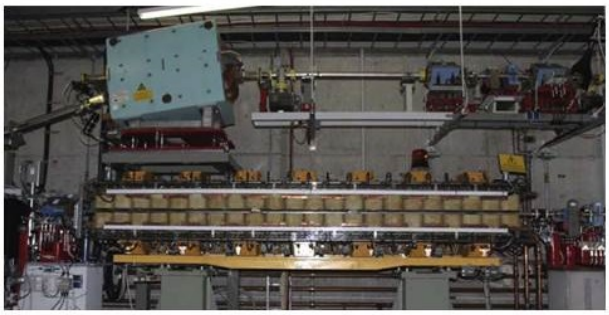

O. Grimm, N.Morozov, A.Chesnov, Y.Holler, E.Matushevsky, D.Petrov, J. Rossbach, E.Syresin , M.Yurkov, NIMA 615 (2010) 105

Fig. 9: The THz undulator for FLASH

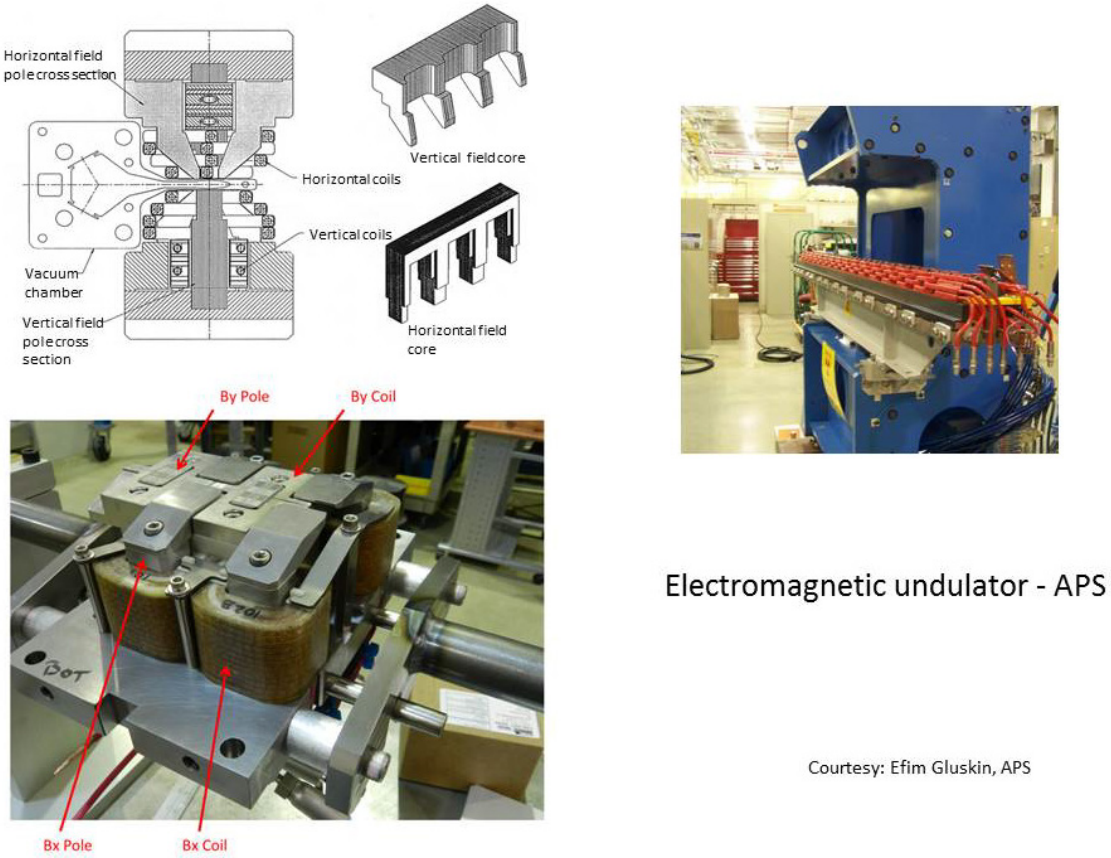

Fig. 10: EM helical undulator for the APS

3.3 SC devices

The technological advantages of SC devices were already described in Section 3.1. As an example of long-period/high-field devices Fig. 11 shows the wavelength shifter built for Spring8. It has a magnetic length of about 1 m only and accommodates just three poles. The central pole is designed for highest field and reaches up to 10.2 T. It is surrounded by two side poles with lower field and longer length, which balance and control the first and second field integrals. The field distribution is seen in the lower left of Fig. 11. At 8 GeV this device is used to create ultra-hard X-rays with a critical energy of 440 keV, which should be compared with about 64 keV from a conventional bending magnet at 1.5 T. In general wavelength shifters are good choices if the spectrum of X-rays emitted by bending magnets is too soft. An example: in a typical soft X-ray storage ring with 2 GeV the critical photon energy of a conventional 1.5 T bending magnet is about 4 keV only. This is much too low for special X-ray techniques such as protein crystallography, which requires photon energies of about 24 keV (0.5 Å). With a 10.2 T wavelength shifter as described above the critical energy is shifted to 27 keV.

The technology for these devices is well established and used in many storage rings throughout the world.

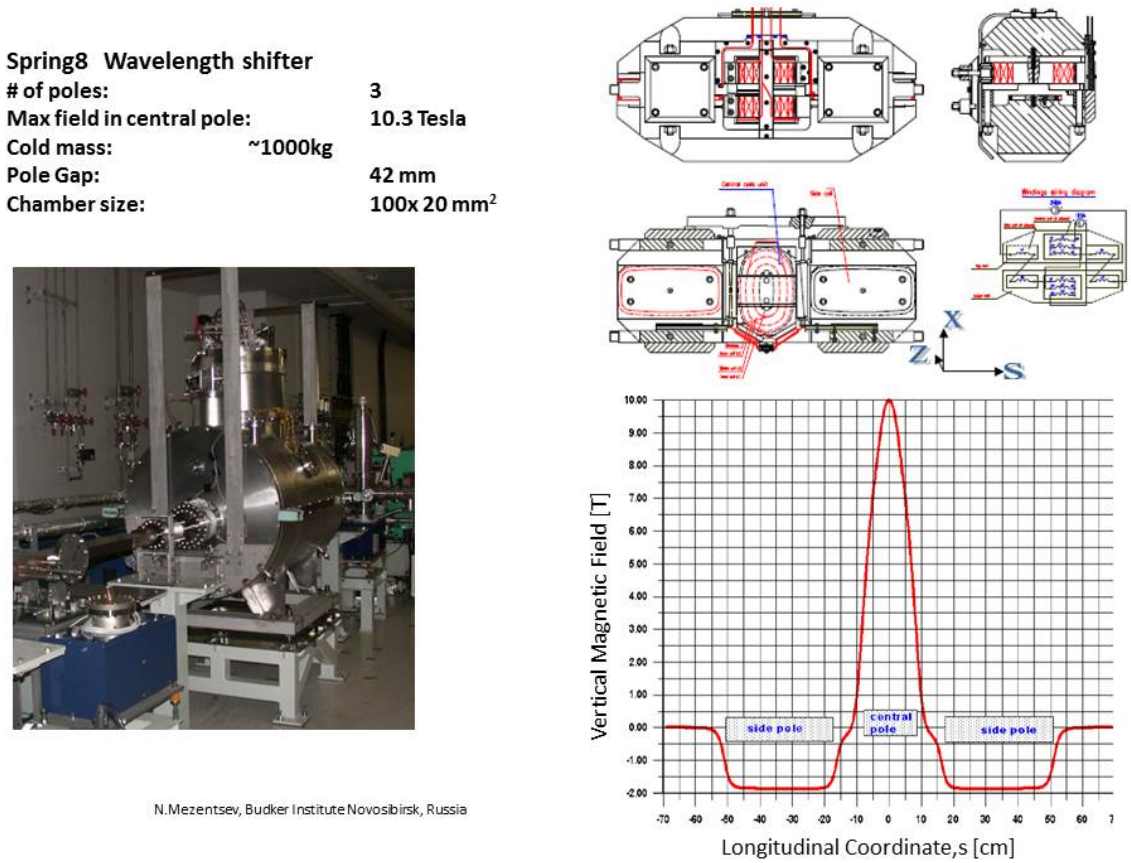

Fig. 11: The SC wavelength shifter built by BINP for Spring8

For short-period SC undulators the situation is quite different. Two examples are shown in Fig. 12. The upper one was built for the Anstroemquelle Karlsruhe (ANKA) at the Karlsruhe Institute of Technology (KIT) and is in operation since 2005. The lower one is a short prototype under development for the APS upgrade. It has only 20 periods and a magnetic length of about 300 mm but is inserted in a full-size 2 m cryostat, the planned final length of the device.

This device is part of a systematic development at the APS. The plan is to use a large number of SC devices for the planned upgrade of the APS storage ring expected to start in 2020. It will be the first large-scale use of SC undulators.

Some of the technological challenges which need to be solved are briefly mentioned.

i) Proper radiation shielding is required to prevent heat load from SR originating from upstream magnets especially in long small-gap devices.

ii) A vacuum chamber is needed to separate the accelerator vacuum from the cryogenic part, which reduces the usable gap.

iii) Magnetic measurements in such a device require substantial effort.

iv) There is no compensation scheme for field errors. Field quality can only be guaranteed by perfect manufacturing.

v) The production technology needs to be further developed. At present (2016) it is not yet mature enough to be used for a large number of devices.

The target parameters for the final APS device are: λ_0 = 15 mm; $B_{\mathrm{Peak}} \leq 1.5$ T; $K \leq 2.1$; magnetic gap = 7.3 mm; vacuum gap = 5.0 mm. This should be compared to an in-vacuum hybrid PM device where magnetic and vacuum gaps are the same, that is, 5.0 mm: λ_0 = 15 mm; gap = 5.0 mm: B_{Peak} = 0.82 T; K = 1.15. So peak field and K-parameter of a SC device are significantly larger in spite of the larger magnetic gap of the SC undulator. This demonstrates the advantage of SC technology.

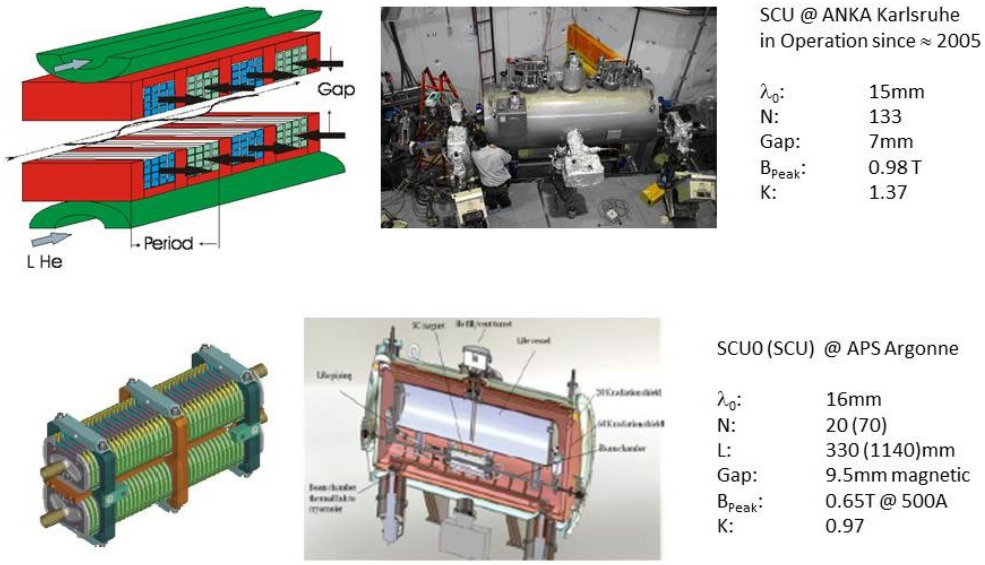

Fig. 12: SC undulator development at ANKA and APS

3.4 PM undulators

3.4.1 Magnet design

New PM materials based on sintered SmCo and NdFeB compounds were developed in the 1970s and 1980s. They offer much higher energy products resulting in higher remanent and coercive fields and therefore much increased magnetic performance as compared to traditional ferrite or AlNiCo materials, which were used before. This development revolutionized many applications using PM technology.

The use of these materials for insertion devices was pioneered by Klaus Halbach, who proposed the two different magnet configurations, which are still used without modification for planar undulators worldwide [7, 8]. The pure permanent magnet (PPM) structure is shown in Fig. 13, left. The structure is assembled from parallelepipeds arranged in two rows and magnetized as shown in the figure. The space between the upper and lower rows is called the 'gap'. By changing the gap mechanically, the field strength in the gap can be accurately controlled. The field of a homogenously magnetized parallelepiped with $\mu_{\mathrm{r}} = 1.0$ can be calculated analytically using the current-sheet method. The field of a complete structure is obtained by superposition of the fields. This is good for many calculations. For precise data, however, the finite permeability μ_{r} needs to be taken into account; $\mu_{\mathrm{r}} \approx 1.05$–$1.07$ for NdFeB and 1.02–1.03 for SmCo.

Obviously the field of a PPM undulator is fully determined by the PM material, its quality, homogeneity, magnetic orientation, mechanical dimensions and manufacturing accuracy. These are important quality criteria and depend on many details of the production process. There might be large variations for commercially available materials.

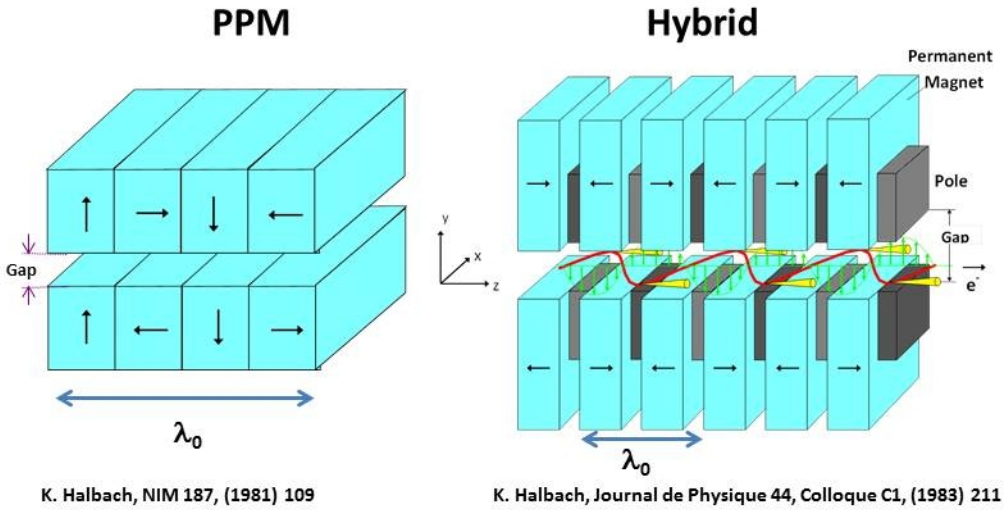

Fig. 13: Left-hand side: PPM array. Right-hand side: hybrid array

An alternative is the hybrid configuration, Fig. 13, right, which avoids some of the drawbacks of the PPM design but requires more effort. It uses a combination of soft iron poles and PM material arranged again in a bottom and a top array with a gap in between. The iron poles concentrate the flux of the magnets and conduct it to the gap. The fields in general are higher than for PPM. In contrast to PPM undulators the field is dominated by the geometry of the poles and only to a lesser extent by material quality. This allows a better and more direct control of field errors as well as eventually some compromises on material quality.

For field calculations of hybrid undulators there are no analytic methods and numeric codes need to be used. Since these codes generally allow for $\mu_r > 1$ they are often used for PPM structures as well. A very popular code in the insertion device community is RADIA developed at the ESRF [9].
Today for most undulator applications NdFeB magnet material is used because it offers the highest energy product. Only for special applications requiring high temperatures or extremely high coercive fields SmCo material is an alternative.

For design work and parameter determination it is very useful to have an analytic formula which describes the peak field as a function of the gap. A convenient form was already given in Ref. [8], see also Ref. [6]:

$$B\left(\frac{g}{\lambda_0}\right)[\mathrm{T}] = a\, \mathrm{e}^{b\frac{g}{\lambda_0}+c\left(\frac{g}{\lambda_0}\right)^2} \tag{32}$$

The normalization to $\lambda_0$visualizes the scaling properties described in Section 3.1. The constants *a*, *b* and *c* are determined by fitting using either calculated or measured data of a specific design and geometry. Using scaling the same magnet design can in principle be scaled to different λ_0.

Figure 14 shows a selection of normalized gap dependencies fitted using Eq. (32). They are taken from the literature as well as from results obtained at DESY and the European XFEL. The coefficients *a*, *b* and *c* are shown in Table 1 for some of the curves shown in Fig. 14. Here are some remarks

1. As expected, the PPM curve is well below the hybrid curve.
2. The majority of the curves are close together. They all use hybrid magnet designs optimized for relatively small period lengths, $\lambda_0 < 48$ mm.
3. In contrast, the curve for BW5 was optimized for a large-period device with $\lambda_0 = 230$ mm. The objective was a high field of about 1.98 T and a gap of 20 mm, gap/$\lambda_0 = 0.087$.

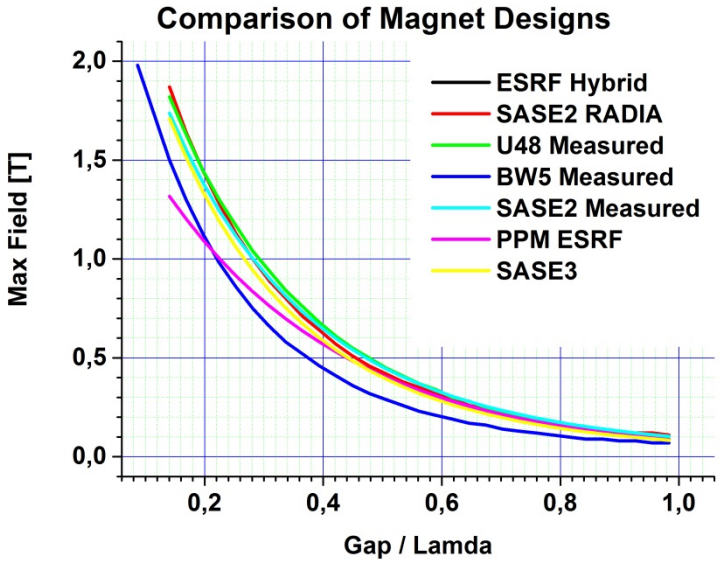

Fig. 14: Examples of gap dependences normalized to $\boldsymbol{\lambda_0}$

Limits to scaling are only set by physical dimensions. Applying scaling from a small to a large period length requires increasing the volume of magnets and poles proportional to the third power. At material cost of 200 to 500 €/kg for magnet material this sets an economic limit for large-period devices, which therefore always are a compromise between magnet volume/cost and achievable field. An example for scaling is given for the DORIS BW5 wiggler: with λ_0 = 230 mm the weight of one magnet block was ≈15 kg. Using the SASE2 design, which would allow for slightly higher fields and scaling, its weight would have to be about 57 kg.

Table 1: Examples for fitting the parameters *a*, *b*, *c* in Eq. (32)

Magnet structure	***a***	***b***	***c***
Hybrid FeCo poles[a]	3.694	–5.068	1.52
XFEL SASE2 measured[b]	3.10487	–4.24914	0.80266
XFEL SASE3 measured[c]	3.2143	–4.62305	0.92541
DORIS III BW5[d]	3.1852	–5.6036	1.6891
PPM[a]	2.076	–3.24	0

[a] See Ref. [6].
[b] Measured data of EXFEL U40; λ_0 = 40 mm.
[c] Measured data of EXFEL U68; λ_0 = 68 mm.
[d] Measured data of DORIS III 2 T wiggler BW5; λ_0 = 230 mm.

For the design of the mechanics of PM undulators, no matter whether they use PPM or hybrid technology, two points are important:

1. The magnets of the top and bottom structures need to be mounted on girders. In the case of the European XFEL the length is 5 m. There are significant attractive magnetic forces between these girders, which need an accordingly massive and stiff support in order to guarantee homogeneous field properties. The sinusoidal magnetic field applies an attractive magnetic 'pressure' between the upper and lower structures, which can be estimated by

$$F[\mathrm{N/m^2}] = \frac{B_0^2[\mathrm{T}]}{4\mu_0} \tag{33}$$

As a rule of thumb, a field of 0.5 T corresponds to about 0.5 bar, which for a 5 m long and 70 mm wide structure amounts to an attractive force of 17500 N. For 1.7 T, which applies to the worst case for the SASE3 undulator for the European XFEL at 10mm gap, it amounts to about 200 kN. Girder stiffness and the supports need to be designed in such a way that under a dynamic load change with these forces the dynamic girder deformation is typically such that the resulting peak to peak homogeneity does not significantly exceed $\frac{\Delta B}{B} \leq 10^{-3}$.

2. The K-parameter of a PM undulator is tuned by the mechanical adjustment of the gap. For X-ray FELs a typical requirement on adjustment accuracy is $\frac{\Delta K}{K} \leq 10^{-4}$. As a result a typical specification on the mechanics, the drive motors, measurement systems and the motion control system is to allow for a gap-adjustment accuracy better than ±1 μm.

3.4.2 Some examples

3.4.2.1 Open C-frame

Figure 15 shows some examples of the C-frame geometry. It is a very common way to arrange the magnet structures. The principle is shown in Fig. 15(a). There is a stiff frame which is a good support for the guide rails, to which the girders are connected to. The gap is adjusted via spindles. Nowadays usually gears are avoided and axes are coupled and synchronized electronically by the control system rather than by hardware such as shafts and gears. There might be four motors, one for each spindle, as seen in the two examples for LCLS II, Fig. 15(b) and the European XFEL, Fig. 15(d) or alternatively two motors in combination with two right/left spindles, as seen in Fig. 15(c), which shows a standard carriage of the ESRF. This device in addition is equipped with four spring systems, which are used for partial compensation of the magnetic forces. The great advantage of the C-geometry is its good access from the open side. This is seen in Fig. 15(d), which shows a 5 m long undulator segment aligned on the magnetic bench. Magnetic measurements and tuning can be done in an alternating fashion. The C-bracket with the hand-off sign seen in the foreground on the end of the girder is part of the gap-measurement system with a verified accuracy of ±1 μm.

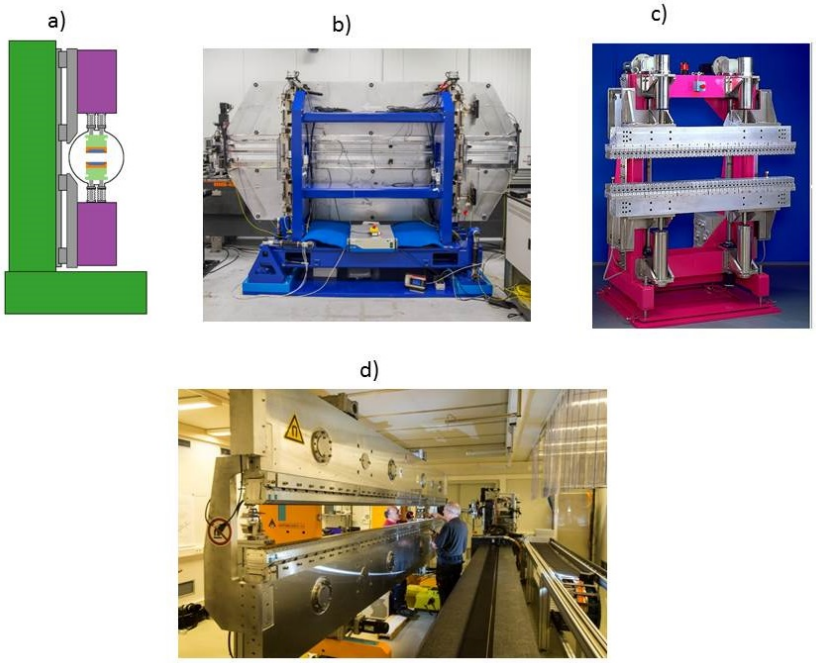

Fig. 15: Undulators with C-frame geometry. (a) Principle; (b) 2.3m LCLS II prototype; (c) 1.6m ESRF standard carriage; (d) A 5m U40 undulator for the European XFEL aligned on the magnetic bench.

3.4.2.2 Revolver undulators

A special case of C-frame devices are revolver undulators. They allow for the use of different magnet structures which are mounted on rotatable drums or girders so they can be changed rapidly. The principle is shown in Fig. 16(a). Different magnet structures are arranged on drums. Different ones can be selected by proper rotation of the upper and lower drums. Figure 16(b) shows the 4 m long BW3 undulator used in DORIS III from 1990 to 2012. It provides four positions. The bearings for the drum rotation need to be at the ends and allow for four positions and continuous rotation.

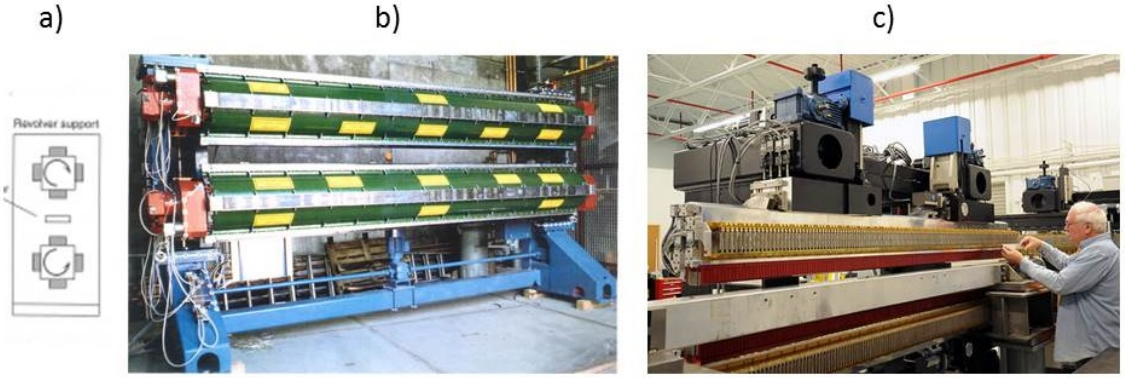

Fig. 16: Revolver undulator. (a) Principle; (b) DORIS III BW3 revolver with four positions; (c) APS revolver with cradle support with two positions.

However, but their locations are non-optimum for mechanical deformation under attractive forces. Enforced drums as well some extra length of about 0.3 m for the bearings on either end are required. Deformation properties can be improved by shifting the support to the Bessel points using cradle-type circular guide rails as seen in Fig. 16(c). But in this case only two structures can be accommodated and continuous rotation is not possible. Revolvers are used in many laboratories to extend the scan range of undulators.

3.4.2.3 H-frame geometry

The H-frame geometry is shown schematically in Fig. 17(a). It uses a symmetric and closed frame and therefore in contrast to the C-frame it is more compact and less prone to deformation. Figure 17(b) shows an early example built in 1987: it is the hard X-ray wiggler (HARWI) used in DORIS III during 1987–2004 for coronary angiography. For highest performance requiring smallest gaps in dedicated SR runs it was equipped with a variable vacuum chamber. Lateral access in H-frame devices is very restricted. Only limited magnetic measurements can be performed. High-precision systems as shown in Fig. 15(d) cannot be used. For these reasons compact H-frame devices as shown in Fig. 17 are rare.

Recently a very slim measurement system was reported, which can be used under such spatial conditions. Although it was built for in situ measurements in in-vacuum undulators, which encounter the same problem, see also next section, it might be a perfect system for the magnetic measurement of H-frame devices as well.

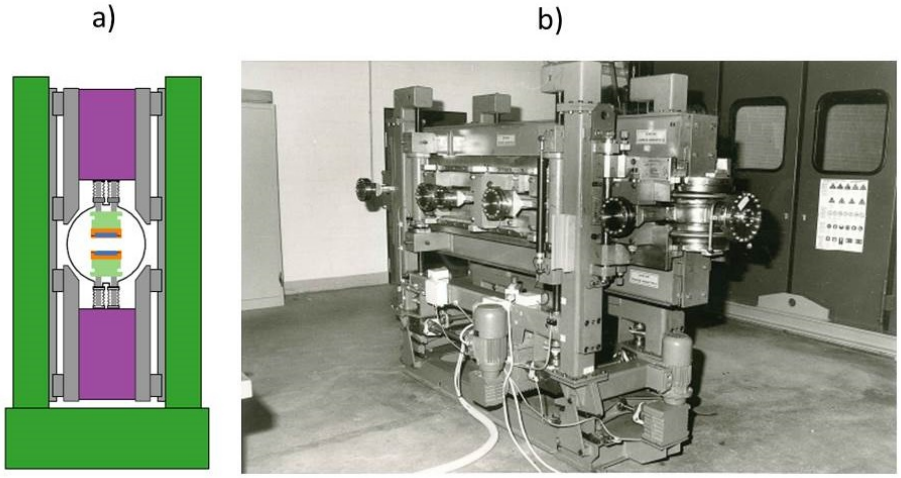

Fig. 17: (a) H-Frame geometry; (b) 2.4 m long Hard X-ray Wiggler (HARWI) used at DORIS III for coronary angiography 1987–2004.

3.4.2.4 In-vacuum undulators (IVUs)

The relativistic electron beam, which is passed through an undulator in order to generate light, needs a vacuum chamber. This aspect has not been treated so far. There exist two alternatives, which are illustrated in Fig. 18. In most undulators a separate vacuum chamber with an aperture as small as possible is used; see Fig. 18(a). Such an out of vacuum chamber requires space for the vacuum chamber wall thickness plus some tolerances. This limits the usable magnetic gap. An example is given in Fig. 18(c). It shows the dimensions of the vacuum chamber for the undulator segments of the European XFEL. It is made of an extruded AlMg alloy, which has been machined to exact final dimensions. The minimum magnetic gap of the undulator is 10.000 mm, the vertical beam stay clear is 8.6 mm and the vertical outside dimension of the vacuum chamber is 9.5 mm. This results in a wall thickness of 0.45 mm only. There is a 0.5 mm tolerance for the chamber to fit in the undulator. However, in this optimized example the usable gap is reduced by 1.4 mm.

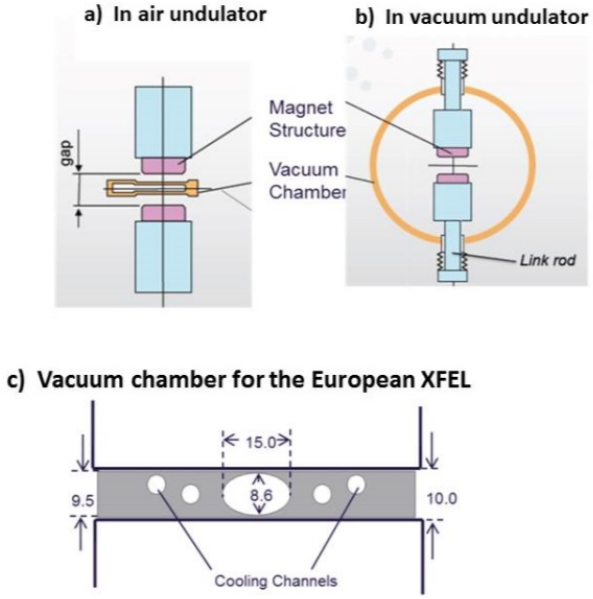

Fig. 18: (a) Conventional out of vacuum chamber; (b) in-vacuum undulator; (c) vacuum chamber of the European XFEL: magnetic gap: 10mm, chamber outside dimension: 9.5mm, alignment tolerance: 0.5mm, beam stay clear: 8.6mm. The resulting wall thickness is 0.45mm only.

An alternative is to place the magnet structure inside the vacuum, Fig. 18(b). In an IVU the magnet structure is completely inside the vacuum chamber and there is no loss in usable gap. There are several problems which should be mentioned.

1. The complete magnet structure needs to be compatible with the ultra-high-vacuum (UHV) conditions of the accelerator.
2. All magnets need special coating in order to prevent outgassing of the sintered magnet material.
3. The whole structure must be designed to avoid virtual leaks.
4. Compatibility with bake out requires selection of adequate magnet material with high H_c.
5. In order to keep the diameter of the vacuum chamber small the magnet structure is supported by a number of link rods. They are connected to a massive external girder using feedthroughs. The assembly of the magnet structures inside the vacuum vessel implies problems with alignment and reproducibility.
6. Magnetic measurements and magnetic tuning are special challenges.

As an example the assembly of an IVU at SACLA is demonstrated in Fig. 19. On the left the pre-assembled IVU is aligned on the magnetic bench without vacuum chamber to provide lateral access for magnetic measurements and tuning. Some of the details already mentioned above are seen: there are the massive external magenta support girders, 12 pairs of link rods with their feedthroughs protected by aluminium foil and there is the very slim magnet structure, which will go inside the vacuum chamber. After measurement and tuning the magnet structure needs to be completely detached from the 2 × 12 link rods, transferred inside the vacuum chamber and re-attached. Obviously there is only finite reproducibility of the re-attachment of the link rods to the girders. This may induce errors in the magnetic field, which would stay undetected if no further steps are made. The final assembled IVU is seen on the right of Fig. 19. The endcap of the vacuum vessel is still opened. Most IVUs in use today use the techniques described above and end at this point.

A big step forward was the development of the self-aligned field analyser with laser instrumentation, (SAFALI) system which allows in situ magnetic measurements; see Ref. [10]. In this way the re-attachment errors can be measured and compensated. Its principle is shown in Fig. 20, left. There is a very slim guide system, which carries the field probe and is supported by three adjustable posts. Their supports go through three flanges in the vacuum vessel. During measurements the probes are kept on axis using two laser positioning systems and feedback loops to adjust the posts in such a way as to keep the probe on axis. This system in operation is seen in Fig. 20, right.

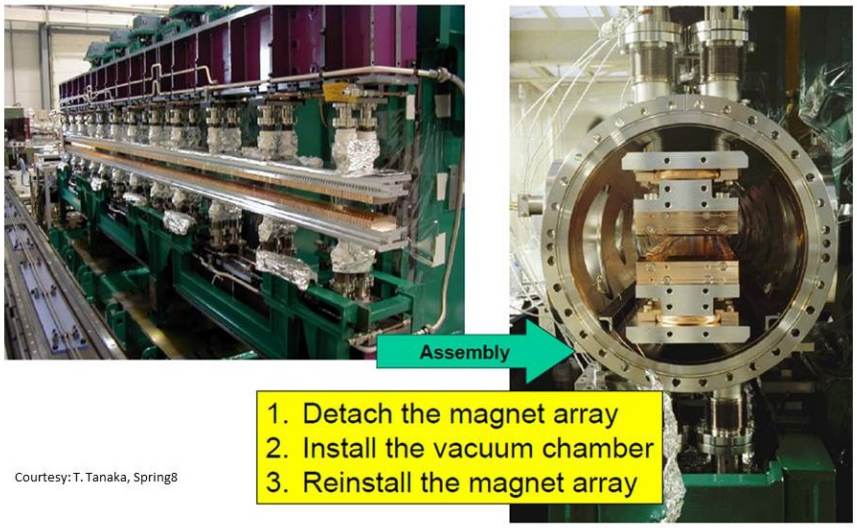

Fig. 19: Magnetic measurement and final assembly of an in-vacuum undulator

Figure 21 shows one of the SACLA IVU systems. It consists of 18 undulator segments of 5 m length. The period length is 18 mm. The minimum operational gap is as small as 3.7 mm and the maximum *K*-parameter is 2.1. At 8 GeV X-rays with a wavelength as short as 1 Å can be produced.

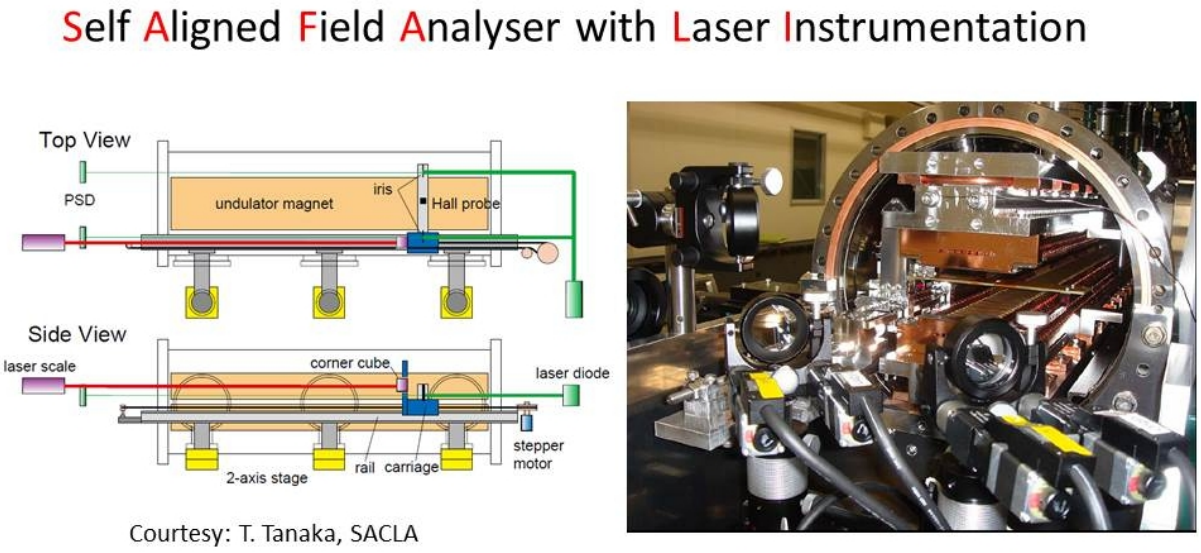

Fig. 20: SAFALI system. Left-hand side: principle; right-hand side: measurement on an IVU

Fig. 21: One of the SACLA IVU systems

3.4.2.5 APPLE undulators

For PPM structures the superposition principle allows the combination of fields produced by different magnet structures. This gave rise to a number of different types of insertion devices, which have been proposed over the years. A full treatment and explanation is beyond the scope of these proceedings. However, one example, the advanced polarized light emitter, APPLE, undulator [11] became popular for spectroscopic applications and is briefly explained. It allows the creation of light with any polarization state: planar, right/left circular, elliptical and planar with arbitrary plane of polarization. The principle is shown in Fig. 22. An APPLE undulator consists of a PPM structure, in which each half is subdivided into two rows. Each row can be moved individually. This is shown schematically in Fig. 22(a). If all rows have the same shift the geometry is equivalent to a PPM undulator and there is only a B_y field component. If the rows are shifted diagonally as indicated in Fig. 22(a) a horizontal field component is generated resulting in elliptical polarization. If the shift is $\pm\lambda_0/4$ helical radiation with right/left helicity is generated. Planar fields can be generated by mutually shifting the diagonal pairs.

An APPLE undulator provides a planar gap and therefore is ideal for storage rings, which require a large horizontal aperture. Its total field is controlled by the gap. The horizontal gap together with the C-frame geometry allows good access for magnetic measurements. However, depending on the shift of the rows there might be large forces, which are not present in planar undulators. Therefore they require substantially enforced massive frames. Figure 22(b) gives an impression. It shows the 5 m long APPLE undulator built for upgraded Positron Electron Tandem Ring Accelerator PETRA III.

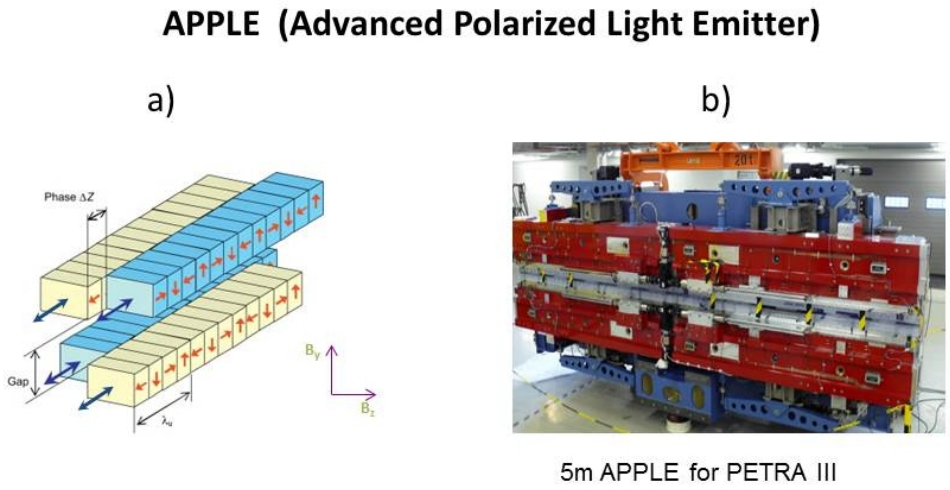

Fig. 22: APPLE undulator

4 Summary and outlook

Undulators are indispensable components in storage rings and in SASE FELs, where they are used in very long systems. In this contribution an overview of the current status of undulator technology is given. The most important parameters such as period length, λ_0, the *K*-parameter, radiation wavelength λ_{Rad} , first and second field integrals, the optical phase and the RMS phase errors were explained.

The three different technologies for building undulators were introduced: EM, SC and PM technologies. Their domains and pros and cons were discussed. Special emphasis was put on PM technology, which is used in the majority of applications.

Stimulated by new accelerator developments, which allow smaller emittances and beam sizes, there is a trend to reduce the undulator gaps to less than 4 mm as in the case of SACLA and SwissFEL. Together with short-period IVUs and beam energies of 5.8 GeV, radiation in the Angström regime and below can be produced. However, a severe limitation for small-gap PM undulators is radiation damage, which is caused by halo electrons and secondary particles colliding with residual gas and vacuum-chamber atoms. Such radiation damage has been observed already in conventional warm accelerators based on copper technology with repetition rates of typically 50–120 Hz but will become much more important for projects using SC accelerators such as the European XFEL or LCLS II, where repetition rates up to the MHz range will be used. Obviously the protection of undulators from radiation damage will be an important challenge for these new projects. It will require elaborate countermeasures such as collimators, doglegs, loss detectors and active protection systems to prepare a well-collimated beam without any contamination from particles outside an allowed, well-defined phase space which may hit the vacuum chamber. Here the minimum gap is a critical parameter.

Once the technology is mature enough SC undulators might be a good choice: at given gap and λ_0 they offer higher fields or alternatively they offer the same field at a significantly larger gap than PM

devices. In addition, the superconductor material NbTi is believed to be much less sensitive to radiation damage than PM material. There are, however, no direct comparative measurements yet.

At present, autumn 2016, PM technology is the method of choice for all applications requiring short period length. This may change once SC technology is mature enough to be used routinely on large-scale systems for SASE FELs. This will require time and stimulation by the requirements of new projects such as the APS upgrade or future LCLS II extensions.

References

[1] H. Onuki and P. Elleaume, *Undulators, Wigglers and their Applications* (Taylor & Francis, New York, 2003). https://doi.org/10.4324/9780203218235

[2] J. Clarke, *The Science and Technology of Undulators and Wigglers* (Oxford University Press, Oxford, New York, 2004).

[3] S. Krinsky, M.L. Perlman and R.E. Watson, in *Handbook of Synchrotron Radiation*, Eds. Y. Farges and E.E. Koch (North Holland, Amsterdam, 1983), Vol. 1, Chap. 2.

[4] R.P. Walker, *Nucl. Instrum. Methods A* **335** (1993) 328. https://doi.org/10.1016/0168-9002(93)90288-S

[5] Y. Li, B. Faatz and J. Pflueger, *Phys. Rev. ST Accel. Beams* **11** (2008) 100701. https://doi.org/10.1103/PhysRevSTAB.11.100701

[6] P. Elleaume, J. Chavanne and B. Faatz, *Nucl. Instrum. Methods A* **455** (2000) 503. https://doi.org/10.1016/S0168-9002(00)00544-1

[7] K. Halbach, *Nucl. Instrum. Methods* **187** (1981) 109. https://doi.org/10.1016/0029-554X(81)90477-8

[8] K. Halbach, *J. Phys. Colloques* **44**(C1) (1983) C1-211. https://doi.org/10.1051/jphyscol:1983120

[9] P. Elleaume, O. Chubar and J. Chavanne, Computing 3D magnetic field from insertion devices, Proc. PAC97 Conf., May 1997, pp. 3509–3511. The code is available under http://www.esrf.eu/Accelerators/Groups/InsertionDevices/Software/Radia

[10] T. Tanaka, T. Seike and H. Kitamura, Measurement of Spring-8 XFEL undulator prototype with the SAFALI system, FEL2009 Proc., 24–29 August 2009, Gyeongju, Korea; see also T. Tanaka, Spring8 EFST on Insertion Devices Workshop, 3–4 December 2009, Shanghai, China, http://www.sinap.ac.cn/meeting/EFST2009/142nd-EFST/EFST_TTanaka.pdf

[11] S. Sasaki, K. Miyata and T. Takada, *Jpn J. Appl. Phys.* **31** (1992) 1794. https://doi.org/10.1143/JJAP.31.L1794